Optimizing Interface Conductivity in Electronics

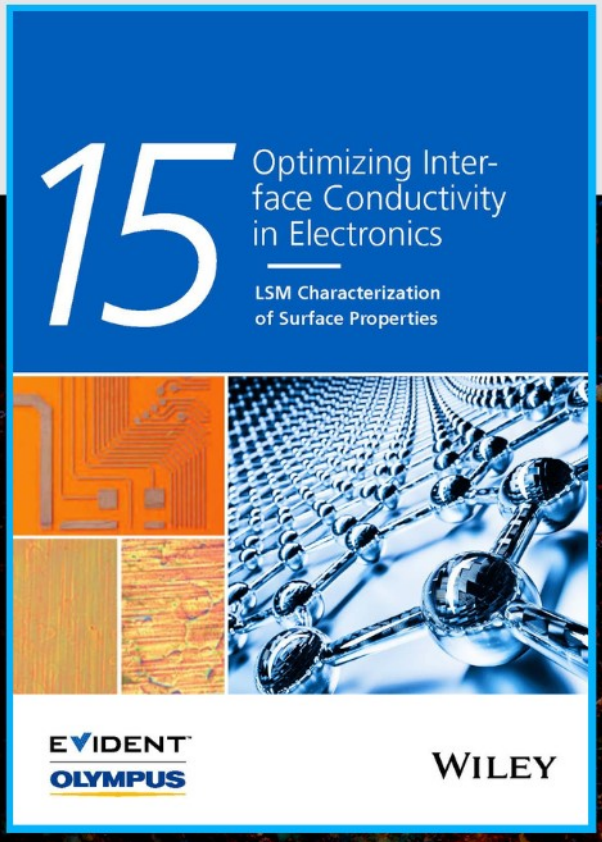

The latest eBook from Advanced Optical Metrology. Download for free.

Surface roughness is a key parameter for judging the performance of a given material's surface quality for its electronic application. A powerful tool to measure surface roughness is 3D laser scanning confocal microscopy (LSM), which will allow you to assess roughness and compare production and finishing methods, and improve these methods based on mathematical models.

Focus on creating high-conductivity electronic devices with minimal power loss using laser scanning microscopy is an effective tool to discern a variety of roughness parameters.

EVIDENT
OLYMPUS

WILEY

ADVANCED ELECTRONIC MATERIALS
Open Access
www.advelectronicmat.de

Configurable NbO_x Memristors as Artificial Synapses or Neurons Achieved by Regulating the Forming Compliance Current for the Spiking Neural Network

Chuan Yu Han, Sheng Li Fang, Yi Lin Cui, Weihua Liu, Shi Quan Fan,* Xiao Dong Huang, Xin Li, Xiao Li Wang, Guo He Zhang, Wing Man Tang, P. T. Lai, Jia Liu, Xianjie Wan, Zhou Yu, and Li Geng*

For the first time, a configurable NbO_x memristor is achieved that can be configured as an artificial synapse or neuron after fabrication by controlling the forming compliance current (FCC). When the FCC ≤ 2 mA, the memristors exhibit the resistive-switching (RS) property, enabling multiple types of synaptic plasticity, including short-term potentiation, paired-pulse facilitation, short-term memory, and long-term memory. When the FCC ≥ 3 mA, the memristors can be electroformed and exhibit the threshold switching (TS) property with excellent endurance (>10^{12}), thus achieving various biological neuron characteristics, such as threshold-triggering, strength-modulation of spike frequency, and leaky integrate-and-fire. This enables the successful implementation of a spiking Pavlov's dog that employs the spikes as information carrier by connecting an RS NbO_x memristor as artificial synapse and a TS memristor as artificial neuron in series. Furthermore, a fully NbO_x memristors-based single-layer spiking neural network is simulated. It is first found that, due to the forgetting property of synapse, the recognition accuracy for the Modified National Institute of Standards and Technology handwritten digits is increased from 85.49% to 91.45%. This study provides a solid foundation for the development of neuromorphic machines based on the principles of the human brain.

1. Introduction

With the advent of the big data era, the amount of data has exploded, bringing huge computing demands.[1–5] The traditional Von Neumann computing architecture increasingly suffers from the "memory wall" problem where significant energy cost and wire delay are caused by frequent data flow between the central processing unit and the memory.[6–8] In contrast, the human brain is very efficient with an average power consumption of only 20 W.[9] Therefore, the neuromorphic spiking neural network (SNN) that mimics the working mode of human brain has attracted significant interest. To effectively implement neuromorphic SNN directly in hardware, two basic electronic components must be developed: the artificial synapses and the artificial neurons. However, due to the lack of inherent dynamic characteristics, lots of metal oxide semiconductor field effect transistors are used to construct a single synapse or neuron, thus increasing the complexity of neuronal and synaptic circuits, making it difficult to obtain large integration scale comparable with that of human brain.[10–12] Hence, developing novel electronic devices with intrinsic dynamic properties and scalability to construct efficient neuromorphic machines has received extensive attention recently.

Memristors have the advantages of simple structure, scalability, fast switching speed, fault tolerance, low power consumption, and compatibility with complementary metal oxide semiconductor process, rendering them ideal hardware units to break the Von Neumann bottleneck and realize efficient

C. Y. Han, S. L. Fang, Y. L. Cui, W. Liu, S. Q. Fan, X. Li, X. L. Wang, G. H. Zhang, L. Geng
School of Microelectronics
Xi'an Jiaotong University
Xi'an 710049, P. R. China
E-mail: hanchuanyu@xjtu.edu.cn; junjunfan@mail.xjtu.edu.cn

The ORCID identification number(s) for the author(s) of this article can be found under https://doi.org/10.1002/aelm.202300018.

DOI: 10.1002/aelm.202300018

X. D. Huang
Key Laboratory of MEMS of the Ministry of Education
School of Electronic Science and Engineering
Southeast University
Nanjing 211189, China

W. M. Tang, P. T. Lai
Department of Electrical and Electronic Engineering
The University of Hong Kong
Hong Kong 999077, China

J. Liu, X. Wan, Z. Yu
No.24 Institute
China Electronics Technology Group Corporation
Chongqing 404100, P. R. China

neuromorphic computing.[13–16] Recently, multiple types of biological synaptic plasticity are realized by using resistive-switching (RS) memristors,[17–19] and various biological neuronal functions have been achieved based on threshold-switching (TS) memristors.[20–22] However, most of the reported memristors exhibit only RS or TS properties. If the switching properties of a memristor can be configured after the fabrication, the fabrication process of neuromorphic chip will be greatly simplified and the integration scale greatly enhanced. Due to the abundance of chemical valence states of niobium (Nb), NbO_x memristors can exhibit both RS and TS properties by controlling the oxygen contents.[19,23–26] Thus, it is highly possible to enable the simultaneous realization of various synaptic plasticity and neuronal functions in a single NbO_x memristor. For example, Liu et al. demonstrated a $Pt/NbO_2/Pt$ device for TS property and a $Pt/Nb_2O_5/Pt$ device for RS and obtained a hybrid characteristic by connecting these two devices in series.[27] Luo et al. reported a 3D $TiN/TiO_2/NbO_x/Pt$ device with RS and TS property before and after the forming process.[28] Although the reported devices exhibit the characteristics of RS and TS property, they do not possess the synaptic behaviors or neuronal properties.

In this work, a NbO_x memristor with the structure of $Ti/W/NbO_x/Nb/Pt$ can be configured as the artificial synapse or artificial neuron by regulating compliance current during the forming process (forming compliance current (FCC)). The memristors have excellent consistency, low forming voltage (≈4.2 V), and good endurance (>10^{12}). When the FCC ≤ 2 mA, the memristors exhibit multiple types of biological synaptic plasticity, including short-term potentiation (STP), paired-pulse facilitation (PPF), short-term memory (STM), and long-term memory (LTM). Meanwhile, when the FCC ≥ 3 mA, the memristors show various biological neuronal behaviors, such as threshold-triggering, strength-modulation of spike frequency, leaky integrate-and-fire (LIF), and refractory period. Based on the artificial synapses and neurons implemented by the configurable NbO_x memristors, employing the spikes as information carrier, a spiking Pavlov's dog was successfully implemented in hardware and a fully connected single-layer SNN was set up to recognize the Modified National Institute of Standards and Technology (MNIST) handwritten digits with the recognition accuracy of 91.45% by simulation, thus providing a solid foundation for the realization of neuromorphic machines.

2. Results and Discussion

2.1. Characterization of NbO_x Memristors

As shown in **Figure 1**a,b, the memristors were fabricated on SiO_2/Si wafer, employing a via-hole (≈10 µm) structure of

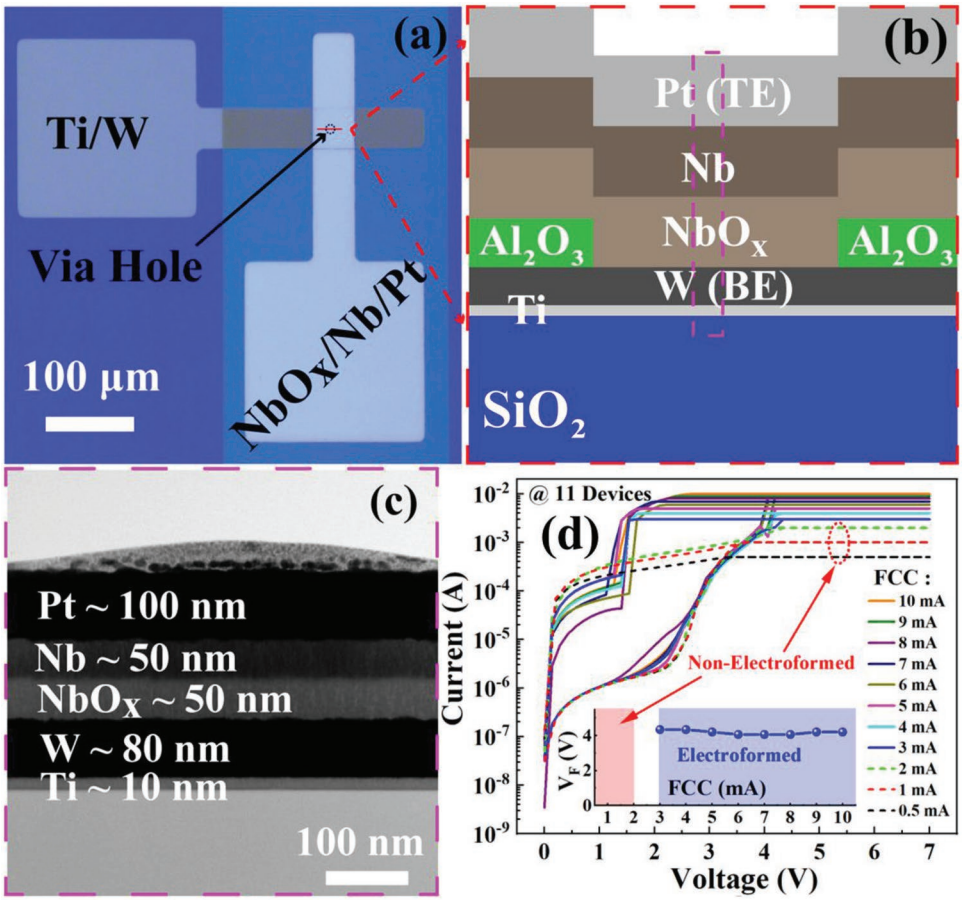

Figure 1. a) Optical micrograph, b) schematic diagram, and c) cross-section TEM image of the fabricated NbO_x memristor. d) Forming processes of 11 devices under different FCCs and the inset is the distribution of the forming voltage (V_F).

Ti/W/NbO_x/Nb/Pt crossbar. The cross-section transmission electron microscope (TEM) images of the memristor are shown in Figure 1c and Figure S1a in the Supporting Information. The as-deposited NbO_x is amorphous as determined by the electron diffraction pattern (see Figure S1d, Supporting Information).

As shown in Figure 1d, when the FCC ≤ 2 mA, the currents of the NbO_x memristors have large hysteresis windows without abrupt change during the forming process, exhibiting RS property, thus the devices are configured as artificial synapses whose conductance can be modulated by applied voltage pulses. Meanwhile, when the FCC ≥ 3 mA, the currents of the memristors change abruptly and the memristors are electroformed, showing the TS property, thus the devices are configured as the artificial neurons that can generate oscillating spikes under proper driven current or voltage. As shown in the inset of Figure 1d, the forming voltages of eight devices (FCC ≥ 3 mA) are all distributed around 4.2 V, indicating the good consistency of forming process.

2.2. Synaptic Plasticity of the Configured Artificial Synapse

As shown in **Figure 2**a and Figure S2a–c in the Supporting Information, when the device is configured as the artificial synapse with the FCC ≤ 2 mA, the backward current of the memristor gradually decreases and forward current gradually increases as the cycle number of the positive DC voltage sweeps increased, thus the hysteresis window gradually decreases, suggesting that the conductance of the memristor can be gradually modulated under voltage pulses. Then, the devices were measured under different voltage pulses as shown in the inset of Figure 2b. Under 30 positive voltage pulses (4.5 V/0.1 s set, 0.5 V/0.1 s read, I_{CC} = 2 mA, the set compliance current during pulse measurement), the conductance of the memristors gradually decreases, and under 30 negative voltage pulses (–4.0 V/0.1 s reset, 0.5 V/0.1 s read, I_{CC} = 2 mA), the conductance gradually increases to the initial highest conductance state. The conductance of the memristor can be repeatedly increased or decreased by applying positive or negative pulse trains, thus successfully simulating the depression and potentiation plasticity of biological synapse. The variations in the conductance of different synaptic devices are shown in Figure S2d in the Supporting Information, indicating that the configured artificial synapses have good consistency.

To construct an SNN, multiple types of synaptic plasticity, including STP, PPF, STM, and LTM[29,30] are emulated by using the configured artificial synapses. As shown in Figure 2c, when a single presynaptic voltage pulse (4.5 V/0.1 s, I_{CC} = 2 mA) is applied, a sharp increase in current (excitatory postsynaptic current, EPSC) is observed, but then the EPSC rapidly drops back to its initial value after the removal of the applied voltage pulse, thus realizing the STP. When two paired voltage pulses (4.5 V/0.1 s, interval of 0.5 s, I_{CC} = 2 mA) are applied, the EPSC of the second voltage pulse (A2) is higher than that of the first pulse (A1), hence the device exhibits the PPF with the strength A2/A1 of 1.7 (Figure 2d). As shown in **Figure 3**, the transition from STM to LTM can be achieved by applying consecutive voltage pulses. When a few pulses (–4.0 V/0.2 s, I_{CC} = 2 mA)

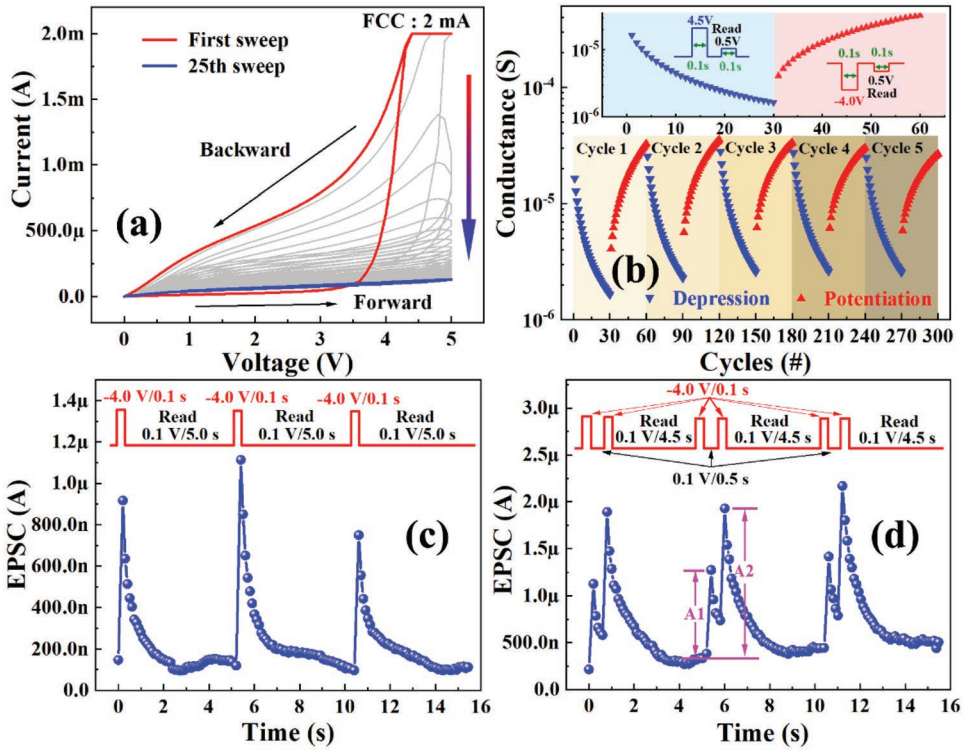

Figure 2. a) 25 *I–V* curves under repeated positive DC voltage sweeps with FCC = 2 mA for a typical device. b) Depression and potentiation plasticity of NbO_x memristors. Inset is the conductance plasticity under 30 positive and 30 negative pulses, respectively, and the corresponding applied voltage pulses. c) STP. d) PPF.

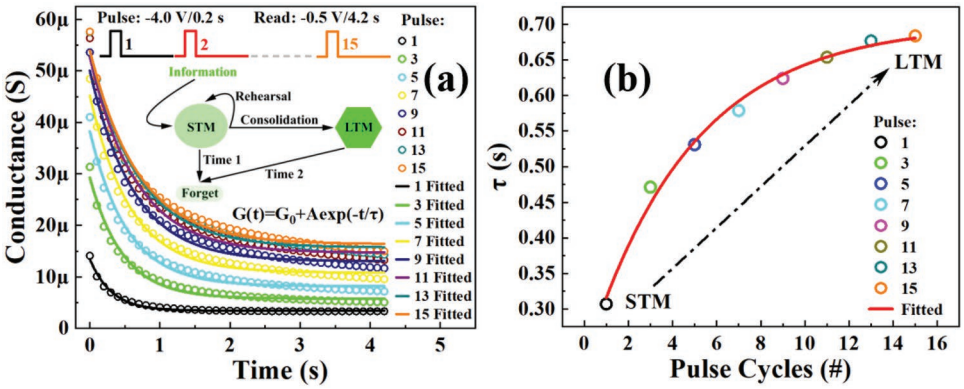

Figure 3. a) Experimental (symbols) and fitted (solid lines) retention property of the NbO_x memristor device after subjected to different voltage pulse cycles. Inset is the applied voltage pulse trains (I_{CC} = 2 mA). b) Relationship between the τ and the pulse cycles.

applied, the conductance of artificial synapse quickly decreases to its initial state after the removal of the applied pulse(s), which is the forgetting property of the artificial synapse. The good endurance of the forgetting property is shown in Figure S3 in the Supporting Information. With the number of applied pulses increased, the conductance gradually increases and remains at high level for long time after removal of applied pulses (see Figure 3a), indicating that the transition from STM to LTM is successfully achieved. More details on retention time of synaptic weights are shown in Figure S4 in the Supporting Information.

In order to accurately describe the forgetting property of the configured artificial synapses, the relation between the relaxation time constant (τ) that evaluates the forgetting speed of the artificial synapse and synaptic weight (G) can be obtained by fitting the retention curve with the modified Kohlrausch equation,[31] expressed by

$$G(t) = G_0 + A\exp(-t/\tau) \quad (1)$$

where $G(t)$ and G_0 are the synaptic weights retained at the time of t and at the stabilized state, respectively, and A is the pre-exponential factor. As shown in Figure 3b, with the number of pulses increased, the τ gradually increases, suggesting that the synaptic weight can be maintained at high level for long time.

2.3. Artificial Neuron Achieved by the NbO_x Memristor

When the FCC is set at 5 mA, the as-fabricated NbO_x memristors were electroformed and successfully configured as TS memristor as shown in Figure S5 in the Supporting Information. The compliance current during pulse measurement (I_{CC}) is set to 1 mA. Figure S6 in the Supporting Information shows a distinct region of negative differential resistance during DC current sweeping after forming process. The forming processes of 15 devices are shown in Figure S7 in the Supporting Information, illustrating that the devices have good consistency of device-to-device variation. The current–voltage (I–V) curves of 50 DC voltage sweeps after forming process were characterized as shown in **Figure 4**a. The I–V curves of different sweeps nearly overlap with each other, and V_{th} changes slightly with the cycles while the V_{hold} is fixed, indicating the good cycle-to-cycle variation. As shown in Figure S8 in the Supporting Information, after 10^4 back-and-forth DC voltage sweeps, the I–V curves of NbO_x memristor after forming process nearly show no change, and through the oscillation test shown in the inset in Figure S9a in the Supporting Information, the memristor operated at least 10^{12} times in 10^6 s, proving that the devices have good endurance. Thanks to the TS characteristics of NbO_x memristors, an artificial neuron (leaky integrate-and-fire neuron) is realized as shown in the inset of Figure 4b. When an input voltage (V_{in}) of 6 V is applied, output spikes can be obtained at V_C (V_O) as shown by the blue (red) curve in Figure 4b. When the V_{in} is below 4.0 V, the no output spikes are observed. After the V_{in} increased to 4.5 V, output spikes are generated at V_C (V_O), resembling to the threshold-triggering properties of biological neurons[32] (see Figure 4c). When the V_{in} is increased from 4.5 to 8.0 V, the frequency of output spikes at V_C (V_O) is linearly increased, which bears a resemblance to the strength modulation of spike frequency of biological neurons, i.e., the output spike frequency of neurons increases with the increase of input stimulation.[33,34] The endurance of the strength modulation of the spike frequency function of the NbO_x neurons is shown in Figure S10 in the Supporting Information.

The LIF model of a single neuron greatly simplifies the neural activity to a combination of two mechanisms: "integrate" and "fire," which catches the primary properties of biological neurons. An LIF neuron can be achieved by using the TS NbO_x memristor. When the voltage pulses with constant amplitude (8 V/0.03 s, interval of 0.02 s) are applied, the capacitor (C) will be charged, and the voltage at V_C is gradually accumulated (integrate or summation) as shown by the blue curve in Figure 4d. When the voltage at V_C reaches the V_{th} of NbO_x memristor, the resistance state of the memristor changes from the high resistance state (HRS) to the low resistance state (LRS), and thus a spike is generated at V_O (fire). When outputting a spike, the TS NbO_x memristor is in the LRS, so the C cannot be charged (refractory period). When the V_{in} is removed, the charge on C will gradually leak through the resistor (R_m) (leaky). Thus, an LIF neuron is obtained, whose behavior is similar to that of biological neurons. The relationship between the spikes firing frequency of the LIF neuron and amplitude/duration of the input voltage pulse is shown in Figures S11 and S12 in the Supporting

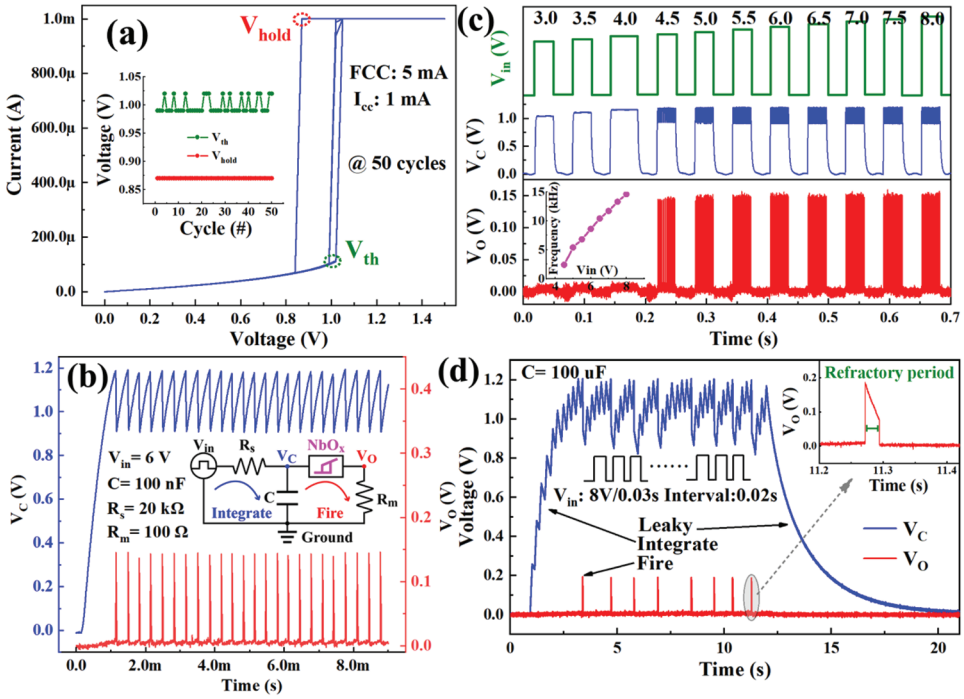

Figure 4. a) 50 cycles of DC sweeps of the NbO_x TS memristor after forming process. Inset is the distribution of V_{th} and V_{hold} over the 50 cycles. b) Oscillating spikes obtained at the V_C (blue) and V_O (red). Inset is the oscillation circuit based on NbO_x memristor. c) Relationship between oscillating spikes rate and V_{in}. Inset is the spiking frequency versus V_{in}. d) Voltage variation of V_C and V_O under voltage pulses input. Circuit for testing is the same as inset in (b), but the capacitance is changed to 100 µF. Inset is enlarge view of one spike.

Information, respectively. With the increase of amplitude/duration of the input voltage pulse, the spiking frequency gradually increases. Therefore, an artificial neuron based on the configurable NbO_x memristor is successfully constructed for the SNN.

2.4. Spiking Pavlov's Dog

The associative learning, an important type of learning process generally existing in biology, refers to that two stimuli happen very close and finally form a connection in the brain, such as the famous classical conditioning Pavlov's dog experiment[35] as shown in **Figure 5**a. Here, the Pavlov's dog experiment is successfully implemented by the configurable NbO_x memristors as artificial synapse and neuron (see Figure 5c) with the learning and testing conditions illustrated in Figure 5b. As shown in Figure 5d, before learning, the RS NbO_x memristor (artificial synapse) was in HRS, and V_O had no spikes output when 6 V voltage pulse as input. After the artificial synapse was trained by using 30 voltage pulses (–4 V/0.2 s, I_{CC} = 2 mA), the artificial synapse is in LRS, and when the voltage pulse (6 V, I_{CC} = 2 mA) is used as input again, spikes can be generated by the TS NbO_x memristor (artificial neuron) at the V_O (see Figure 5e), thus realizing the associative learning.

2.5. Working Mechanism of the Configurable NbO_x Memristors

The conductance of NbO_x can be modulated by the ratio of Nb/O (the lower the Nb/O, the worse the conductivity of NbO_x).[36] The possible working mechanism of NbO_x memristor is shown in **Figure 6**a,b. When FCC ≤ 2 mA, we can see that the devices cannot be electroformed from the *I–V* curves (Figures 1d and 2a), and there is no change in the TE of device before and after voltage sweep (see Figure S13a, Supporting Information). Therefore, we can safely conclude that the drift of oxygen vacancies in NbO_x under the electric field leads to the change of its resistance state due to the change of Nb/O ratio,[28] thus realizing the artificial synapses. When FCC ≥ 3 mA, the device is electroformed with an abrupt current change (see Figure 1d) and a distinct "black spot" appears on the TE of device (see Figure S13b, Supporting Information), proving that a NbO_2 conductive filament (CF) is formed locally in NbO_x due to the high temperature during the electroforming process, results in the abrupt change of the resistance state as illustrated in Figure 6c,d. The NbO_2 filament undergoes the Mott insulator-metal transition under applied voltage and is switched between the insulator phase (i.e., HRS) and metal phase (i.e., LRS),[37] thus enabling the realization of the oscillating neurons.

To verify the working mechanism of the NbO_x memristors, the reduction of synaptic weight for the NbO_x synapse and variation of *I–V* curves for the NbO_x TS memristor under different temperatures were measured as shown in **Figure 7**. As shown in Figure 7a, the higher the temperature is, the worse the memory of the NbO_x synapses. This is consistent with the fact that the speed of oxygen vacancy migration in the NbO_x increased with the temperature increased. Therefore, the realization of the synaptic plasticity is mainly attributed to the oxygen vacancy migration in the NbO_x. As shown in Figure 7b, the resistance

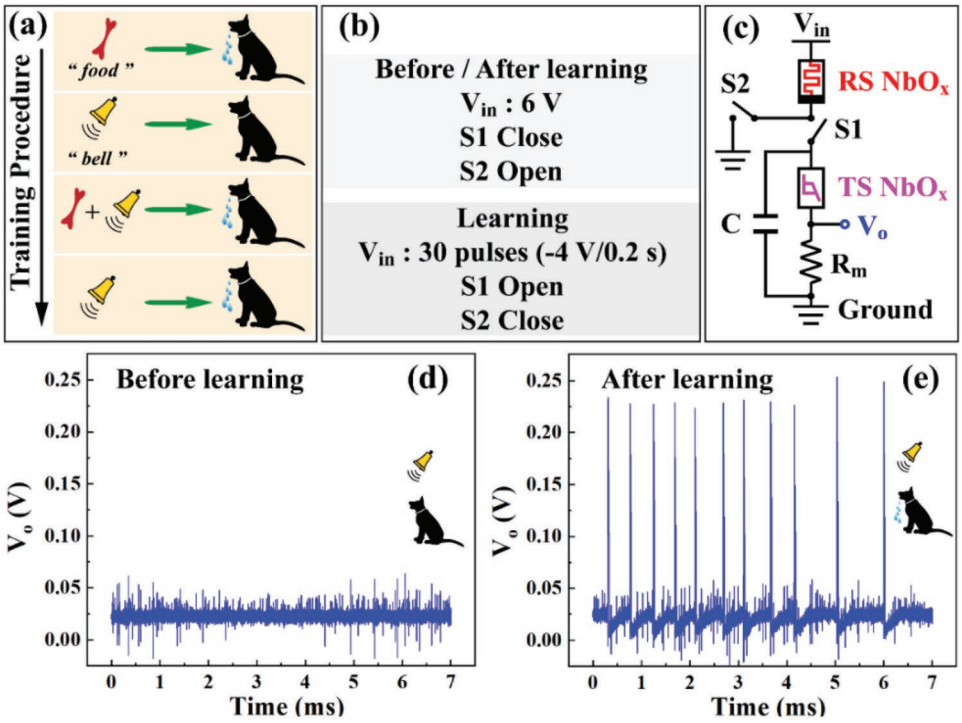

Figure 5. Spiking Pavlov's dog. a) Schematic of the training process for Pavlov's dog. b) Learning and testing conditions. c) Electric circuit with the NbO_x memristors to demonstrate the associative learning. Outputs of V_O d) before and e) after learning.

of HRS and LRS decreases and the memory window (V_{th}–V_{hold}) shrunk with the temperature increased. The resistance of Mott memristor depends on the temperature with an abrupt change at the transition temperature, therefore, with the ambient temperature rising, the resistance of HRS and LRS decreases, and the required Joule heat generated from the applied voltage to reach the transition temperature of NbO_2 decreases, thus the *I*–*V* curve of the NbO_x TS memristors shifts to the left. In sum, the temperature-related study reveals that the synaptic memory properties of configured artificial synapse is attributed to the drift of oxygen vacancies in NbO_x under the electric field, and the threshold switching property of the electroformed NbO_x memristors results from the locally formed NbO_2 CF, enabling the various neuronal functions of TS NbO_x memristors.

2.6. SNN based on the Configurable NbO_x Memristors

Recently, Pickett and Williams developed a coupled electro-thermal physical model to accurately describe the steady-state

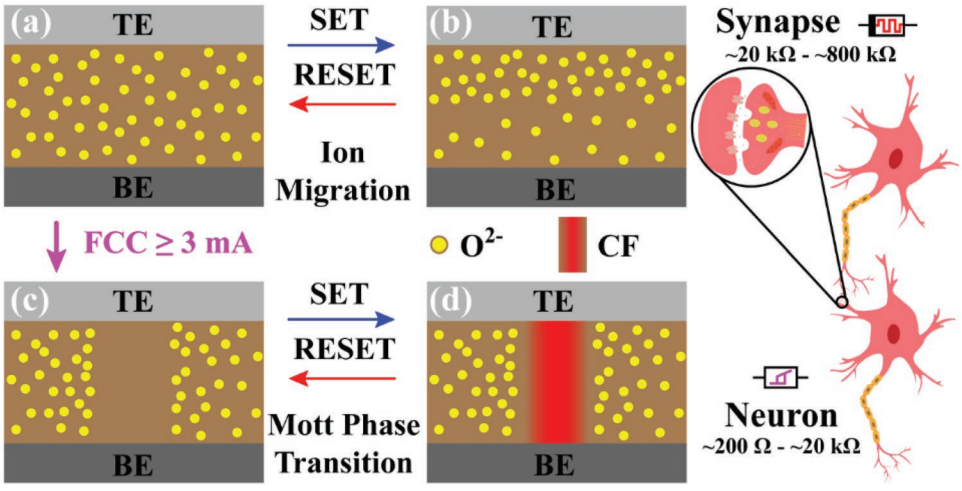

Figure 6. Working mechanism of the NbO_x memristors. a,b) Schematic diagrams of ion migration under the electric field for FCC ≤ 2 mA. c,d) Schematic diagrams of Mott phase transition after forming process.

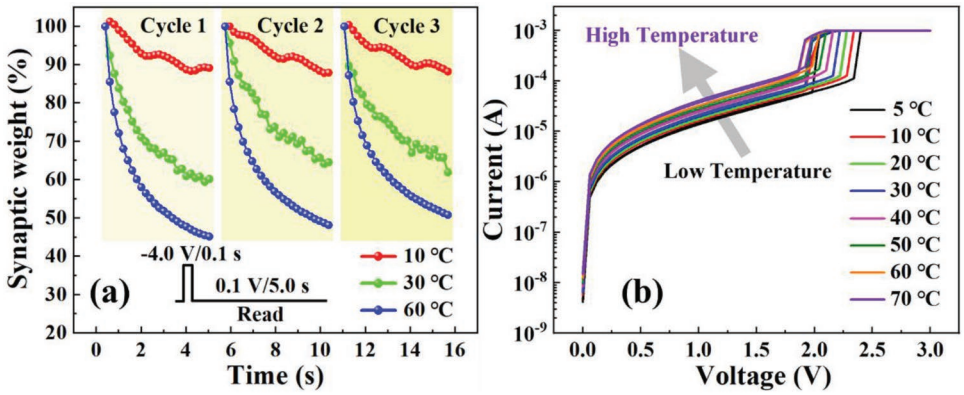

Figure 7. a) Reduction of synaptic weight under different temperatures for NbO_x synapses. b) *I–V* curves of the electroformed NbO_x TS memristors under different temperatures.

I–V relationships and dynamic switching features observed in nanoscale NbO_2.[38] Based on the work, the neuron behavior of the NbO_x memristors was modeled using SPICE. The modeling process and parameters we used are shown in Equations (S1)–(S5) and Table S1 in the Supporting Information. As shown in Figure S14 in the Supporting Information, the simulated *I–V* curve fits well with the experimentally measured data, thus providing a guarantee for the construction of NbO_x memristor-based SNN.

A single-layer fully connected SNN can be achieved for the MNIST handwritten digit recognition by using the synapse array based on RS NbO_x memristors and neurons based on TS NbO_x memristors as shown in **Figure 8**a (more details are referred to the Note S1, Supporting Information). The synapse array is trained offline using 900 MNIST handwritten digits by Python simulator and the training results are shown in Figure S15 in the Supporting Information. The trained positive and negative synaptic weights in hardware are achieved by additional amplifiers (conversion circuits) and the neurons are constructed by connecting a TS memristor with a capacitor and a resistor as shown in Figure 8a. The simulated recognition accuracy of MNIST handwritten digits gradually increases as the number of training epoch increases (see Figure 8c). After 100 epochs, the recognition accuracy can reach 85.49%, assuming that synaptic weights do not change over time during training, i.e., without synaptic forgetting training. Considering that NbO_x memristors

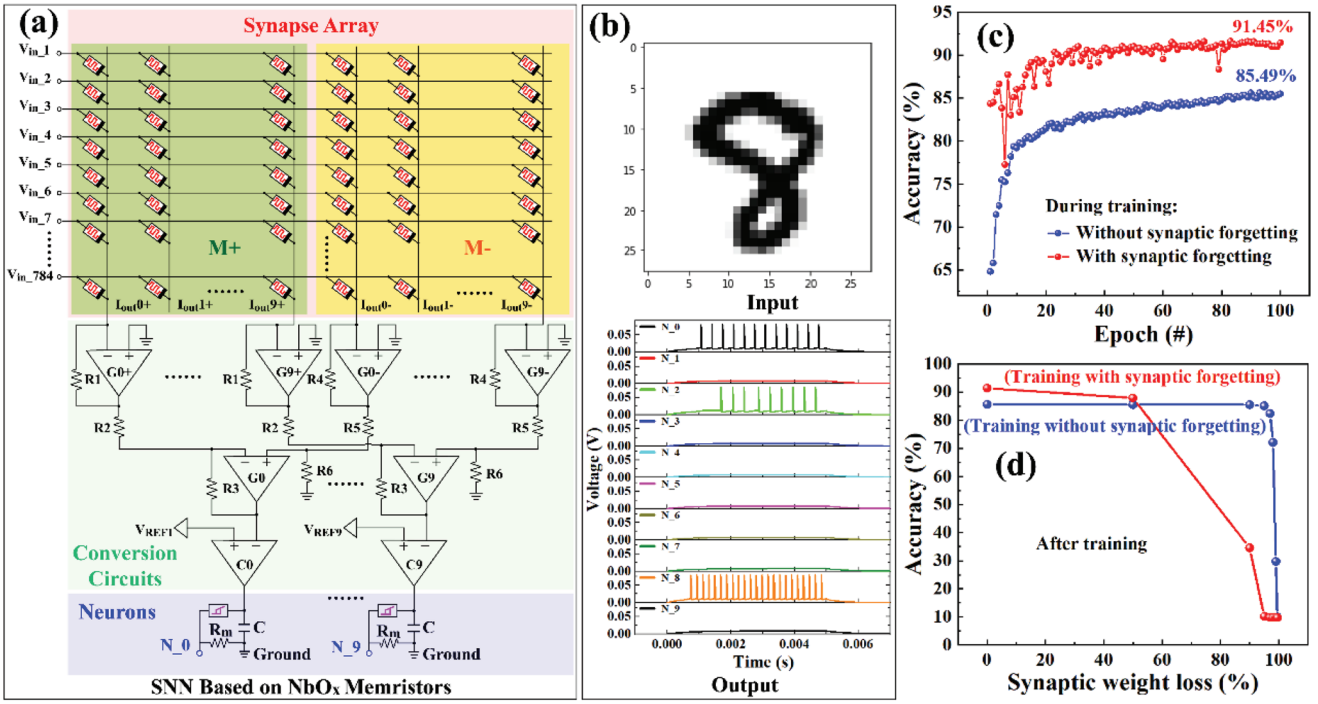

Figure 8. Training and testing on the MNIST handwritten digit recognition by simulation. a) A single-layer fully connected SNN based on NbO_x memristors. b) Recognition process of a typical handwritten digit "8" from the MNIST database. c) Recognition accuracy of the MNIST handwritten digits with and without the synaptic forgetting property. d) Relationship between recognition accuracy and degradation of synaptic weights over time.

used as artificial synapses have the forgetting property, the simulated recognition accuracy is revealed to be increased to 91.45% after 100 epochs, i.e., synaptic forgetting training (see Figure 8c). The increase of recognition accuracy is attributed to that the synaptic array quickly forgets unimportant weights, thus making larger weights more important. As a result, the recognition accuracy of SNN is significantly increased when the forgetting characteristics of synapses is considered in the SNN. Figure 8d shows the relationship between recognition accuracy and degradation of synaptic weights over time. Assuming that all synaptic weights degenerate over time at the same rate after the training, when the synaptic weights lost 50%, the recognition accuracy of SNN with/without forgetting property does not change, but when the synaptic weights lost 90%, the recognition accuracy of SNN with the forgetting property dramatically decreases. The simulation results demonstrate that the introduction of the forgetting property can greatly improve the recognition accuracy, at the same time degrade the stability of the SNN over time.

3. Conclusion

In conclusion, the functions of biological synapse and neuron are realized by controlling FCC of the memristor with the structure of Ti/W/NbO_x/Nb/Pt. The memristors have good consistency and low forming voltages. When FCC ≤ 2 mA, the memristors exhibit multiple types of biological synaptic plasticity, including STP, PPF, STM, and LTM. Meanwhile, when the FCC ≥ 3 mA, the memristors show various biological neuronal behaviors, including threshold triggering, strength-modulated spike frequency, and LIF property. Based on the artificial synapses and neurons implemented by the NbO_x memristors, the Pavlov's dog experiment was successfully realized and an SNN was set up to recognize the MNIST handwritten digits with the recognition accuracy of 91.45%, hence, providing a solid foundation for the realization of neuromorphic machines.

4. Experimental Section

Device Fabrication: The fabrication process was as follows. First, the Ti/W (≈10 nm/80 nm) bottom electrode (BE) was deposited by a radio frequency magnetron sputterer and then patterned by using the lift-off process. After that, the Al_2O_3 (≈30 nm) as isolation layer was prepared and patterned. Finally, the NbO_x (≈50 nm) as switching layer, and Nb/Pt (≈50 nm/100 nm) as top electrode (TE) were also sputtered and then patterned by using the lift-off process. The detailed parameters of magnetron sputtering for each layer are as listed in **Table 1**.

Measurement: All the electrical measurements were conducted in air at room temperature by an Agilent 4155C semiconductor parameter analyzer and a Keysight B2901A precision source/measure unit. The DC bias was applied to the TE while the BE was grounded.

SNN Simulation: The single-layer fully connected SNN for the handwritten digit recognition was built in Python based on experimental results using SpikingJelly.[39] The synapse array was trained offline using surrogate gradient method. The simulated SNN was composed of 784 input, 7840 synapses, and 10 output neurons which corresponded to 10 handwritten digits (from 0 to 9). TS NbO_x devices were used as LIF neurons of SNN where the parameters were extracted from experimental data. The main parameters of the LIF neuron used in the simulation are V_{th} (1.2 V), V_{hold} (0.8 V), and neuronal membrane potential decay time constant (τ = 100). Surrogate gradient method was used to train the neural network online. Here, the relaxation time constant $\tau_{synapse}$ = 35. 7840*2 RS NbO_x devices could be used to store synaptic weights in hardware. The probability of spikes could be calculated in each time step by comparing the spiking frequency with the length of the simulation time step. The higher the frequency was, the greater the probability of spiking at each time step. The index of the most frequently spiking neuron was taken as a prediction result. Other parameters used in this simulation were batch size = 100, timesteps = 200, SNN learning rate = 1e-3, and training epoch = 100.

Table 1. The detailed parameters of magnetron sputtering for each layer.

Layer	Target	Sputtering pressure	Sputtering ambiance	Thickness
Al_2O_3	Al_2O_3	0.8 Pa	Ar/O_2: 24/1 sccm	30 nm
Ti	Ti	0.8 Pa	Ar: 24 sccm	10 nm
W	W	0.8 Pa	Ar: 24 sccm	80 nm
NbO_x	Nb	0.8 Pa	Ar/O_2: 30/2 sccm	50 nm
Nb	Nb	0.8 Pa	Ar: 24 sccm	50 nm
Pt	Pt	0.8 Pa	Ar: 24 sccm	100 nm

Supporting Information

Supporting Information is available from the Wiley Online Library or from the author.

Acknowledgements

This work was supported by the National Natural Science Foundation of China (grant nos. 62174130, 61704137, 61974026), Key R&D plan of Shaanxi Province (grant nos. 2023-YBSF-407, 2021GY-175, 2022GY-337, 2021JM-019), the Strengthening Basic Disciplines Program (nos. 2022-JCJQ-JJ-1108, 2019-JCJQ-JJ-566), the Fundamental Research Funds for the Central Universities (grant no. xjh012020009), the Opening Project of Key Laboratory of Microelectronic Devices & Integrated Technology, Institute of Microelectronics, Chinese Academy of Sciences.

Conflict of Interest

The authors declare no competing financial interest.

Author Contributions

S.L. contributed to carrying out the measurements, analyzing the data, and writing the paper. C.Y. led the team in the design, measurement, analysis, and writing. Y.L. carried out the SNN simulations and analyzed the data. The manuscript was written with input from all authors and all authors discussed the results.

Data Availability Statement

The data that support the findings of this study are available from the corresponding author upon reasonable request.

ADVANCED ELECTRONIC MATERIALS
Open Access
www.advelectronicmat.de

Keywords

artificial neurons, artificial synapses, forming compliance current, NbO_x memristors, spiking neural networks

Received: January 10, 2023
Revised: February 19, 2023
Published online: April 17, 2023

[1] J. Zhu, T. Zhang, Y. Yang, R. Huang, *Appl. Phys. Rev.* **2020**, *7*, 011312.
[2] Y. Zhang, Z. Wang, J. Zhu, Y. Yang, M. Rao, W. Song, Y. Zhuo, X. Zhang, M. Cui, L. Shen, R. Huang, J. J. Yang, *Appl. Phys. Rev.* **2020**, *7*, 011308.
[3] J. D. Kendall, S. Kumar, *Appl. Phys. Rev.* **2020**, *7*, 011305.
[4] Q. Xia, J. J. Yang, *Nat. Mater.* **2019**, *18*, 309.
[5] K. Roy, A. Jaiswal, P. Panda, *Nature* **2019**, *575*, 607.
[6] A. Sebastian, M. L. Gallo, R. Khaddam-Aljameh, E. Eleftheriou, *Nat. Nanotechnol.* **2020**, *15*, 529.
[7] W. Zhang, B. Gao, J. Tang, P. Yao, S. Yu, M.-F. Chang, H.-J. Yoo, H. Qian, H. Wu, *Nat. Electron.* **2020**, *3*, 371.
[8] M. A. Zidan, J. P. Strachan, W. D. Lu, *Nat. Electron.* **2018**, *1*, 22.
[9] I. K. Schuller, R. L. Stevens, R. E. Pino, M. J. Pechan, *Neuromorphic Computing-From Materials Research to Systems Architecture Roundtable,* USA **2015**, https://doi.org/10.2172/1283147.
[10] G. Indiveri, B. Linares-Barranco, T. Hamilton, A. van Schaik, R. Etienne-Cummings, T. Delbruck, S.-C. Liu, P. Dudek, P. Häfliger, S. Renaud, J. Schemmel, G. Cauwenberghs, J. Arthur, K. Hynna, F. Folowosele, S. Saïghi, T. Serrano-Gotarredona, J. Wijekoon, Y. Wang, K. Boahen, *Front. Neurosci.* **2011**, *5*, 73.
[11] S. Hwang, J. J. Lee, M. W. Kwon, M. H. Baek, T. Jang, J. Chang, J. H. Lee, B. G. Park, *J. Nanosci. Nanotechnol.* **2020**, *20*, 3117.
[12] A. Shaban, S. S. Bezugam, M. Suri, *Nat. Commun.* **2021**, *12*, 4234.
[13] S. Choi, J. Yang, G. Wang, *Adv. Mater.* **2020**, *32*, 2004659.
[14] D. Kim, I.-J. Kim, J.-S. Lee, *Adv. Intell. Syst.* **2021**, *3*, 2000206.
[15] R. Yang, H.-M. Huang, X. Guo, *Adv. Electron. Mater.* **2019**, *5*, 1900287.
[16] T. Zhang, K. Yang, X. Xu, Y. Cai, Y. Yang, R. Huang, *Phys. Status Solidi RRL* **2019**, *13*, 1900029.
[17] M. Wang, Y. Luo, T. Wang, C. Wan, L. Pan, S. Pan, K. He, A. Neo, X. Chen, *Adv. Mater.* **2021**, *33*, 2003014.
[18] X. Mou, J. Tang, Y. Lyu, Q. Zhang, S. Yang, F. Xu, W. Liu, M. Xu, Y. Zhou, W. Sun, Y. Zhong, B. Gao, P. Yu, H. Qian, H. Wu, *Sci. Adv.* **2021**, *7*, eabh0648.
[19] W. Wang, R. Wang, T. Shi, J. Wei, R. Cao, X. Zhao, Z. Wu, X. Zhang, J. Lu, H. Xu, Q. Li, Q. Liu, M. Liu, *IEEE Electron Device Lett.* **2019**, *40*, 1407.
[20] K. Wang, Q. Hu, B. Gao, Q. Lin, F. Zhuge, D. Zhang, L. Wang, Y. He, R. H. Scheicher, H. Tong, X.-S. Miao, *Mater. Horiz.* **2021**, *82*, 619.
[21] H. Liu, T. Wu, X. Yan, J. Wu, N. Wang, Z. Du, H. Yang, B. Chen, Z. Zhang, F. Liu, W. Wu, J. Guo, H. Wang, *Nano Lett.* **2021**, *21*, 3465.
[22] D. Lim, K. Cho, S. Kim, *IEEE Electron Device Lett.* **2021**, *42*, 649.
[23] X. Zhang, Y. Zhuo, Q. Luo, Z. Wu, R. Midya, Z. Wang, W. Song, R. Wang, N. K. Upadhyay, Y. Fang, F. Kiani, M. Rao, Y. Yang, Q. Xia, Q. Liu, M. Liu, J. J. Yang, *Nat. Commun.* **2020**, *11*, 51.
[24] Q. Wu, B. Dang, C. Lu, G. Xu, G. Yang, J. Wang, X. Chuai, N. Lu, D. Geng, H. Wang, L. Li, *Nano Lett.* **2020**, *20*, 8015.
[25] P.-H. Chen, C.-Y. Lin, T.-C. Chang, J. K. Eshraghian, Y.-T. Chao, W. D. Lu, S. M. Sze, *ACS Appl. Mater. Interfaces* **2022**, *14*, 2343.
[26] J. Xu, H. Wang, Y. Zhu, Y. Liu, Z. Zou, G. Li, R. Xiong, *Appl. Surf. Sci.* **2022**, *579*, 152114.
[27] X. Liu, S. M. Sadaf, M. Son, J. Park, J. Shin, W. Lee, K. Seo, D. Lee, H. Hwang, *IEEE Electron Device Lett.* **2012**, *33*, 236.
[28] Q. Luo, X. Zhang, J. Yu, W. Wang, T. Gong, X. Xu, J. Yin, P. Yuan, L. Tai, D. Dong, H. Lv, S. Long, Q. Liu, M. Liu, *IEEE Electron Device Lett.* **2019**, *40*, 718.
[29] W. Xu, S.-Y. Min, H. Hwang, T.-W. Lee, *Sci. Adv.* **2016**, *2*, 1501326.
[30] T. Chang, S.-H. Jo, W. Lu, *ACS Nano* **2011**, *5*, 7669.
[31] G. Liu, C. Wang, W. Zhang, L. Pan, C. Zhang, X. Yang, F. Fan, Y. Chen, R.-W. Li, *Adv. Electron. Mater.* **2016**, *2*, 1500298.
[32] W. Gerstner, W. Kistler, R. Naud, L. Paninski, *Neuronal Dynamics: From Single Neurons to Networks and Models of Cognition*, Cambridge University Press, Cambridge **2014**.
[33] C. Chen, Y. He, H. Mao, L. Zhu, X. Wang, Y. Zhu, Y. Zhu, Y. Shi, C. Wan, Q. Wan, *Adv. Mater.* **2022**, *34*, 2201895.
[34] L. Tang, Y. Huang, C. Wang, Z. Zhao, Y. Yang, J. Bian, H. Wu, Z. Zhang, D. W. Zhang, *J. Mater. Chem. C* **2022**, *10*, 14695.
[35] Q. Hu, Y. Xu, Y. Zhou, S. Wang, Q. Huang, J. Zhao, X. Liang, *ACS Appl. Electron. Mater.* **2022**, *4*, 974.
[36] J. Aziz, H. Kim, S. Rehman, J.-H. Hur, Y.-H. Song, M. F. Khan, D.-k. Kim, *Mater. Res. Bull.* **2021**, *144*, 111492.
[37] P. Chen, X. Zhang, Z. Wu, Y. Wang, J. Zhu, Y. Hao, G. Feng, Y. Sun, T. Shi, M. Wang, Q. Liu, *IEEE Trans. Electron Devices* **2022**, *69*, 2391.
[38] M. D. Pickett, R. S. Williams, *Nanotechnology* **2012**, *23*, 215202.
[39] W. Fang, Y. Chen, J. Ding, D. Chen, Z. Yu, H. Zhou, Y. Tian, Other Contributors, Spikingjelly, **2020**, https://github.com/fangwei123456/spikingjelly (accessed: November 2022).